J. Membrane Biol. 36, 311–335 (1977)

Dynamic Properties of Polyelectrolyte Calcium Membranes

Li-Yen Mae Huang* and Robert A. Spangler

Department of Biophysics, State University of New York at Buffalo, Amherst, New York 14226

Received 1 February 1977

Summary. Shashoua observed spontaneous oscillations in a polyelectrolyte membrane formed by interfacial precipitates of polyacid and polybase. We have here undertaken experimental and theoretical studies of polyglutamic acid-Ca^{++} membrane in order to clarify the processes involved in this dynamic behavior. We find a region of distinct hysteresis in the voltage current curve for this system. A sharp transition from a state of low membrane resistance to one of high resistance occurs at a current density different from that of inverse transition.

This membrane system is modeled as a two layer structure: a negatively charged layer α made of ionized polyelectrolyte in series with a neutral region β in which the polymeric ionic sites are masked by calcium ion. This structure results in a difference in the transference number for the mobile ions, causing salt accumulation at the interfacial region during a current flow in the α to β direction. This altered salt concentration induces a change of polymeric conformation, which in turn affects the membrane permeability and the rate of accumulation. Based upon nonequilibrium thermodynamic flow equations, and a two-state representation of membrane macromolecular conformation, this model displays a region of hysteresis in the current range of experimental observations.

The search for an analog system potentially useful in studying the mechanisms underlying membrane excitability began many years ago. Teorell [24, 25] first constructed a model membrane consisting of a negatively charged glass filter to separate two electrolyte solutions of different concentrations; and observed a slow oscillation in pressure and membrane potential under a constant current flow. By incorporating alamethicin, monazomycin and excitability inducing material (EIM) in lipid bilayer, investigators [3, 17, 18] noted a region of negative slope in the current voltage curve. The voltage-dependent channel-gating events

* *Present address:* Laboratory of Biophysics, IRP, NINCDS, National Institutes of Health, Bethesda, Maryland 20014.

of these modified bilayer systems have many characteristics observed in natural excitable membrane [4, 5, 6]. Recently, several investigators have shown that slow current oscillations may be induced in iodine-doped polyethylene film, and dioleylphosphate modified millipore filter paper [10, 26].

Natural membranes contain substantial amounts of protein (up to 50% by weight) which have proved to have important roles in active transport, oxidative phosphorylation and photosynthesis [16]. Since the specificity and activity of the protein macromolecules depend upon their three dimensional conformation, changes in conformation and the rates of these changes are conceivably a key element in membrane dynamic function. In the hope of understanding the functional role of the macromolecular components in determining the electrical properties of biological membranes, Shashoua [19] constructed an interesting type of model system by electrophoresing polyanion and polycation components into the pores of a neutral support matrix. A surface interaction between the two oppositely charged polymers results in a film of about 1000 Å thickness. When this film is placed between two identical salt solutions, a voltage difference of appropriate magnitude and polarity can induce spontaneous current oscillation, and the membrane current voltage curve has a negative resistance region [20]. Based on the probable structure of the membrane, Katchalsky [12], and Katchalsky and Spangler [14] have put forward a hypothesis for Shashoua's observations. They proposed that such membrane may consist of a series of three layers: an inner polyamphelytic layer where two constituent polymers form the precipitate, sandwiched between two external opposite charge layers of polyanion and polycation. These two external elements have different perm-selective properties. Thus the application of a potential across the anion-cation composite membrane causes the accumulation of salt in the intramolecular space. This triggers a regenerative process, resulting from the increase in salt concentration and contraction of the macromolecular matrix. The frequency of the oscillation calculated from this model is similar to that observed by Shashoua [20].

We have undertaken a closer look at the $I-V$ characteristics of Shashoua's type of polyglutamic acid-calcium membrane and have developed a detailed theoretical analysis of the instability appearing in this system. From the analysis we elicit the criterion of instability, establish the range of current at which the oscillation may appear, and evaluate the characteristics of polyelectrolyte behavior which is of importance for the manifestation of hysteresis phenomenon.

Materials and Methods

The procedures for making the membranes are similar to that used by Shashoua [21]. Certain modifications were incorporated to improve the reproducibility of the preparation. The membrane is made on a polysebacyl piperazine (pip-8) supporting matrix in which the size and density of the pores are found to affect the electrical characteristics of the membrane. Pores in the matrix are generated and the porosity, to some degree, is controlled by adding a small amount of glycerol ($5-10\,\mu$ 1/100 cc) to the casting solution (0.25% pip-8 chloroform solution) [9].

The matrix is made on a clean microscope glass slide, dipped in the casting solution and then withdrawn at the speed of 25 cm/min by a motor driven mount. The subsequent evaporation of chloroform leaves a thin film on the slide surface.

Interference colors in the film reflection have proved to be a useful index of film thickness. Matrix films suitable for use reflected blue or violet with uniform coloration over a region of at least 1 cm^2. The actual thickness of the matrix is checked by electron micrographs of a platinum shadowed film. Shadowed at a known angle, the membrane thickness is estimated from the length of the shadow image projected in the pore. An example of such micrograph is shown in Fig. 1. In this specific case, the film thickness is 700 Å. The films used in this study were around 500–1000 Å thick. The pore size and porosity of the membrane, determined by direct EM measurement of the unloaded matrix, range from 2000–5500 Å in diameter, and 2–5% of the total film area.

The experimental arrangements are shown in Fig. 2. A supporting matrix membrane is clamped between apertures of two identical glass cells. After the matrix is in place, equal volumes of 5% polyglutamic acid and 0.05 M $CaCl_2$ are simultaneously added into cells *1* and *2*, respectively. A small dc current (0.1 ma/cm^2) is applied with the cell containing $CaCl_2$ positive. Allowing an hour for the electrophoretic migration of both the negatively charged polyglutamic molecules, and Ca^{++} into the pore of the matrix, an

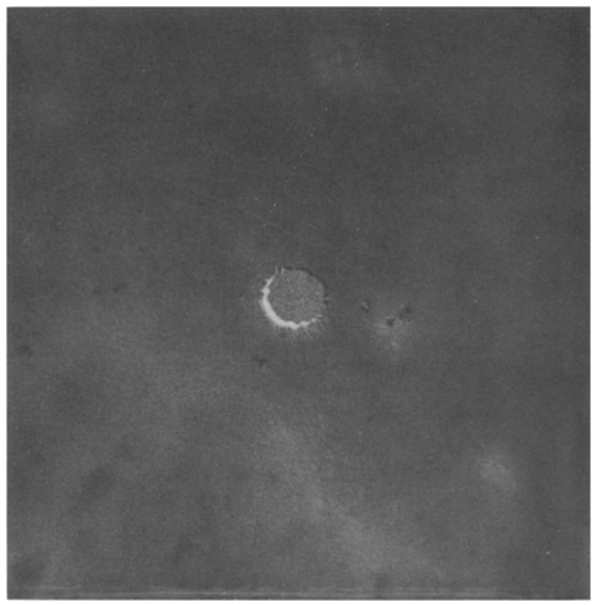

Fig. 1. Electron micrograph of pip-8 matrix. The sample was shadowed at a 45° angle. Using the technique stated in the text, the film thickness in this case is 700 Å

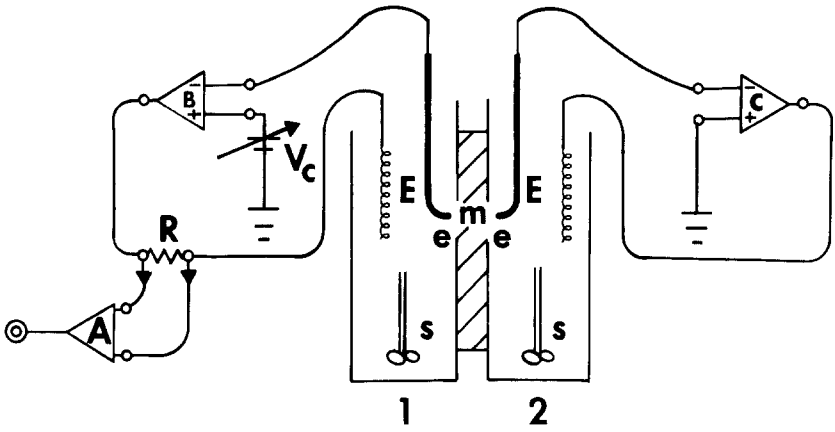

Fig. 2. A scheme of membrane chambers (Cell *1* and Cell *2*) with electronic circuitry for voltage clamp experiment. *E*, current electrode; *e*, voltage electrode; *A*, differential amplifier; *B*, *C*, clamp amplifier; V_c, command voltage; *s*, magnetic stirrer; *R*, 100 Ω resistor; *m*, membrane

asymmetric membrane is formed between the chambers. After washing the polymeric material and Ca^{++} away with KCl solution *in situ*, the chambers are filled with identical solution (e.g., 0.1 M KCl). Two sets of Ag−AgCl electrodes are lowered into the chambers and the membrane is ready for the experiments.

Voltage clamping and current clamping techniques are used to obtain the electrical characteristics of the membrane. The circuit diagram for the voltage clamp experiment is shown in Fig. 2.

Results

The membrane, which remains fairly stable when a small voltage (<0.5 V) is applied, becomes labile upon prolonged application of a transmembrane potential difference beyond the appearance of instability. We, therefore, reversed the polarity of the applied voltage periodically during the course of each experiment, and avoided keeping the membrane voltage above threshold longer than 2–3 min. With such practice, the membrane electrical properties do not change appreciably over 30–40 min.

(a) Oscillatory Phenomenon

Membranes prepared with present method are electrically unstable. Oscillation in the membrane current is observable when the membrane potential is clamped in the range of 0.5–1.3 V. An example of such

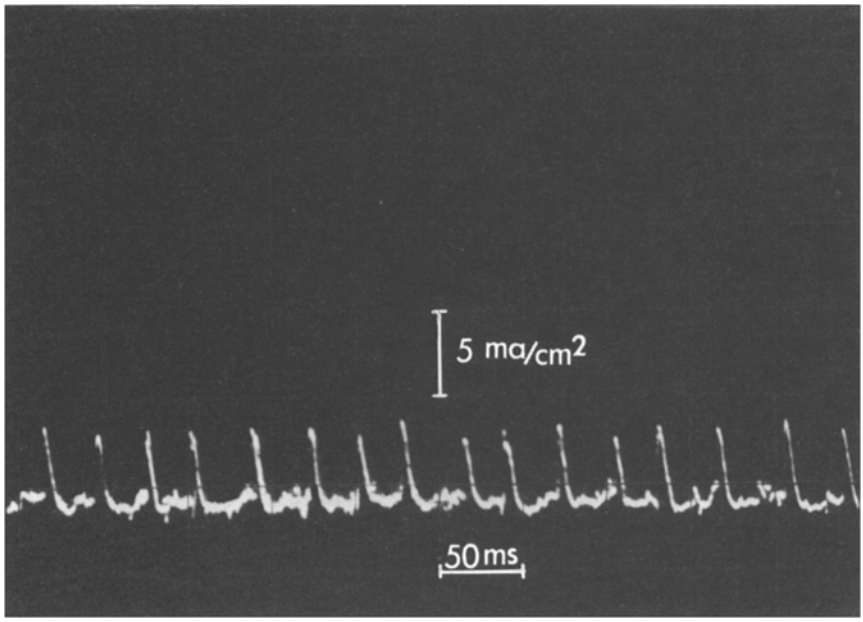

Fig. 3. Oscillatory activity observed in a polyglutamic acid-Ca^{++} membrane. The amplitude scale is 5.0 ma/cm^2, the time scale 50 msec per division

oscillation is shown in Fig. 3. In this case, the amplitude of oscillation is 5 ma/cm^2 with a period of 30 msec. The waveform of the oscillation is asymmetric, having a rising phase of 10 msec and a falling phase of around 20 msec. In general, such oscillation persists only a few minutes before the membrane properties are altered, resulting in the disappearance of oscillatory behavior.

The frequency and amplitude of the oscillatory waveform varies from membrane to membrane. Frequently it assumes the appearance of repetitive short "spike" generation. The frequencies we observed ranged from 20–200 cps with the amplitude varying from 3–10 ma/cm^2. These variations may result from differences in membrane thickness, matrix porosity and other uncontrolled variation in the preparative procedures.

(b) $I-V$ Characteristic Curve

The $I-V$ curves obtained under current clamp differ from that obtained from voltage clamp experiments in the manifestation of the instability, and no oscillation can be detected for the former case. Typical examples are shown in Fig. 4. These curves are nonlinear and asym-

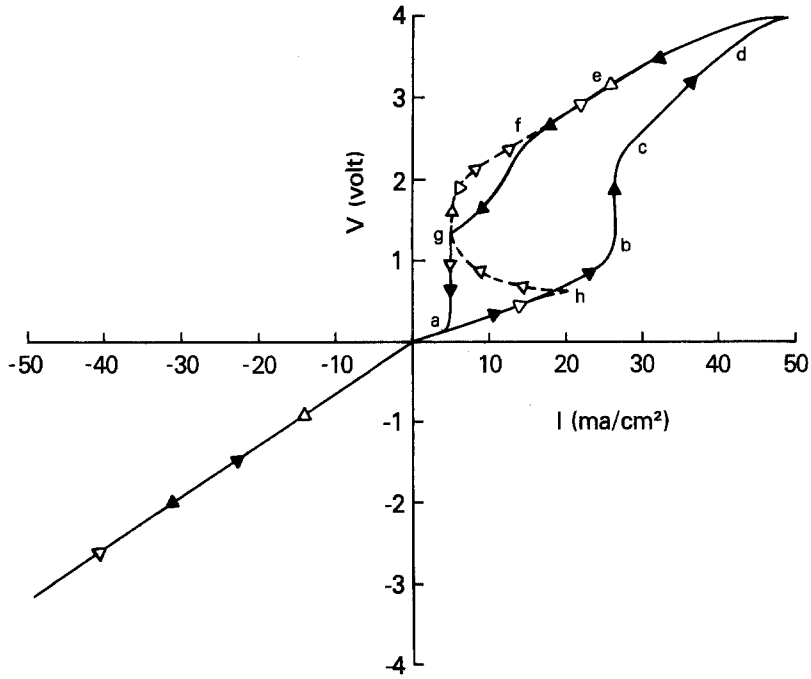

Fig. 4. The voltage-current characteristic curve obtained under V clamp (------) and current clamp (——) conditions. The arrows (▲△) indicate the route taken by the system as the clamp current or voltage is increased and then decreased. Note the presence of two distinct transition regions (corresponding to state *b* and *g*) under current-clamp condition

metric with respect to the direction of current flow and polarity of transmembrane potential.

The solid line is the membrane potential plotted *vs.* the clamp current which varies in a triangular wave fashion. The scanning speed is 0.16 ma/cm^2 sec. The sequential route taken by the system is indicated by the arrows in the diagram. Investigation of membrane characteristics under rigorous steady state conditions is precluded by the limited life span of these membranes. The scanning speed used in this specific case is the slowest feasible. Consequently, the loop generated upon cyclically varying the membrane current represents some degree of residual deviation from steady state conditions. Nonetheless, transient experiments (detailed in Section *c*) demonstrate the existence of two distinct states of the membrane chord resistance. The apparent time constant for the transition between these two states, directly measured, is too small to account for the entirety of the loop apparent in Fig. 4. These observations indicate that the hysteresis loop in the current voltage curve is not simply an artifact of nonsteady state, but a manifestation of the dynamic properties of the membrane system.

The most intriguing feature of this curve is the existence of the two sharp transition regions occurring at different levels of membrane current. The first transition, a change from a state of low chord resistance 39 Ω cm^2 (Point *b*) to one of high resistance 83 Ω cm^2 (Point *c*), appears as the current is increased beyond 26.4 ma/cm^2. The inverse transition (*g* to *a*) does not occur until the membrane current is reduced to 5.1 ma/cm^2.

When membrane properties are measured under voltage clamp conditions, a different characteristic curve emerges. The dotted line represents the result of such experiment. Because of the rapid deterioration of membrane properties during the application of supra-threshold voltage, this curve is recorded with a faster voltage sweep (0.1 V/sec). The membrane current becomes unstable once threshold is reached. The critical voltage is around 0.65 V with corresponding current in the region of 20 ma/cm^2. Superimposed on this dc value, an oscillation in current is triggered. As the voltage is further increased, in addition to the periodic component, the average current starts to drop, ultimately reaching a level of 5 ma/cm^2. The time of transition taken by the system from state *h* to state *g* in this particular case is 7 sec.

The membrane conductance slowly increases to a steady differential value as the clamp voltage scans beyond 2.1 V. The electrical oscillation is lost at these high voltage values. Following decreasing voltage, the changes in conductance take a different course. The current remains practically constant for the voltage level lower than 2.0 V, until state *a* is reached.

The nonlinear behavior and negative differential membrane resistance occur only when the transmembrane potential is positive on the polyglutamic acid side of the membrane (voltage of this polarity is referred as positive hereafter). If the voltage is scanned in a reversed polarity, the membrane current is linearly proportional to its voltage. The corresponding resistance is 78.4 Ω cm^2. With the exception of the unstable region, the voltage clamp and current clamp experiments give consistent $I-V$ relations.

(c) Relaxation Phenomenon

The membrane system behaves as a system with some degree of memory. That is, any instantaneous state of the membrane depends not only on the immediate constraints of the system, but also is some time-dependent function of its history. The history dependence of the system is

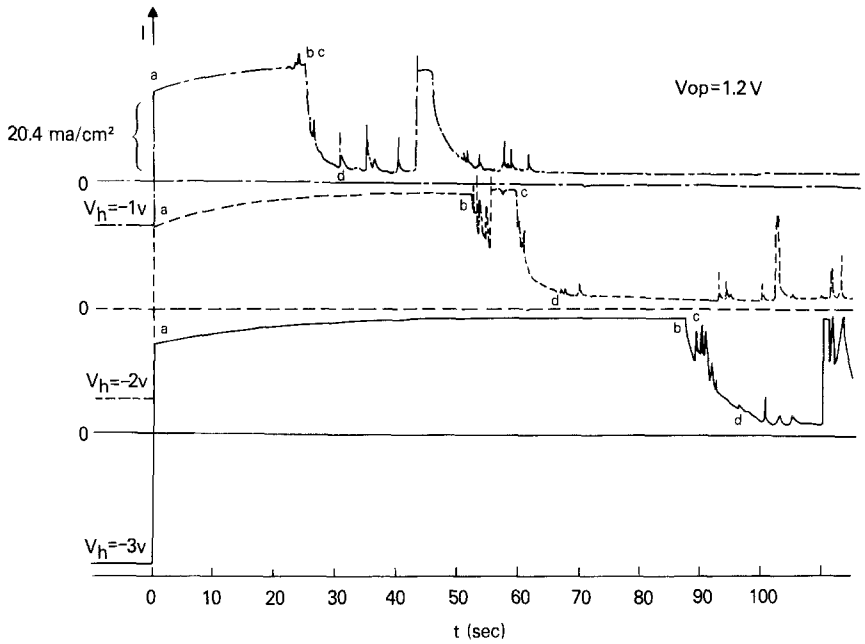

Fig. 5. The relaxation of membrane current as a function of time immediately after the membrane potential is switched from various holding potentials, V_h, to $V_{op}=1.2$ V. ——: $V_h=-3$ V; ------: $V_h=-2$ V; –·–·–: $V_h=-1$ V. t_{a-b} is the latent period prior to the transition. t_{c-d} is the time required for the relaxation process

particularly evident in the hysteresis loop and transition regions of the $I-V$ curve.

The relaxation time constants of the transition process have been measured through observation of the membrane resistance as the system is subjected to a step change in potential (Fig. 5). In these experiments, the test voltage, V_{op}, is chosen around the threshold voltage (i.e., 1.2 V) of the membrane. Immediately following the step change of membrane potential from a holding voltage, V_h to V_{op} the membrane current stays practically constant for a period of time. After this latent period, the current starts to drop sharply, finally reaching a stable high resistance state. The time required for this transition (t_d-t_c) is approximately the same with different holding voltages. Its magnitude, 6–9 sec, is consistent with the result obtained from the $I-V$ measurement (i.e., t_g-t_h in Fig. 4). On the other hand, the delay preceding onset of the transition (t_b-t_a) is approximately linearly proportional to the conditioning voltage. With the membrane conditioned at a more negative value, the transition starts at a later time. In this case (Fig. 5), (t_b-t_a) are 25.0, 52.5, 87.5 sec for the holding voltage of -1, -2, and -3 volts, respectively. As the system

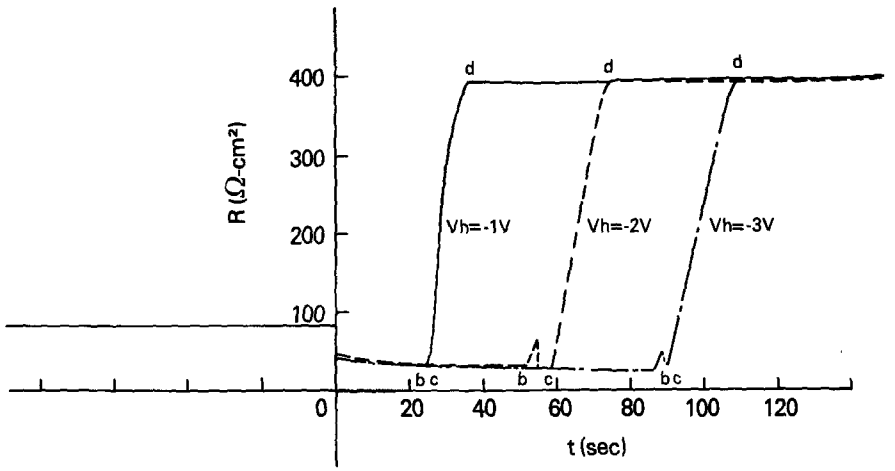

Fig. 6. Time dependence of the membrane resistance obtained under the experimental conditions of Fig. 5

undergoes a transition, it becomes quite unstable and occasionally jumps back to its original state for a very short period of time before it finally reaches the state of high resistance. Transient oscillations of a frequency similar to that of Fig. 3, are also often observed during the transition. When these same experimental results are plotted as resistance *vs.* time (Fig. 6), one finds prior to the switching ($t=0$), the membrane chord resistance remains at $83.2\,\Omega\,cm^2$ regardless of the level of holding voltage.

If V_{op} is set well below the threshold voltage (<0.3 V), the membrane resistance remains constant and no transition is observed in the relaxation curve as expected.

Theoretical Analysis

Since the membranes used in these studies were formed in an ionically asymmetric environment, and exhibited distinct rectification behavior in a symmetric environment, it appears that the structure of the membrane is inhomogeneous and nonsymmetric. We model this complex membrane as a two layer structure: a negatively charged layer α made of ionized polyglutamic acid molecules, in series with neutral layer β where all the ionic sites on the polymeric chains are presumably masked by calcium ions. A schematic illustration of the model is given in Fig. 7.

Because of the fixed negative charges in region α, a major portion of current flow through this layer would be carried by cations. On the other

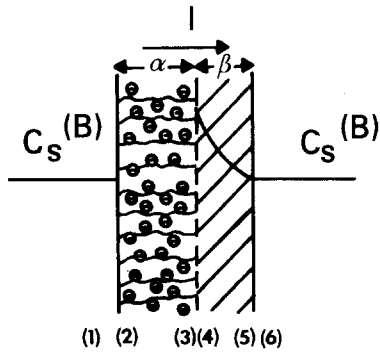

Fig. 7. A schematic illustration of the model for the polyelectrolyte membrane system. The membrane is composed of two elements α and β in series. α is the negatively charged layer, β the neutral layer. Salt will accumulate in β region with the current flow of the direction as indicated in the Figure

hand, in both bulk solutions and the β region, in the absence of exposed fixed charges, cations and anions are assumed to carry equal portions of the current. This difference in transference number causes either accumulation or depletion of salt in the phase boundary regions during current flow. This phenomenon is exaggerated at the right boundary of region α, where stirring is prevented by the presence of the β layer.

Polyelectrolyte molecules assume a highly extended configuration in a low ionic strength solution, and coil up at high ionic strength [11, 13]. Thus during a positive current flow (i.e., polyacid side positive), the polymeric molecules in the α region are expected to undergo a conformational transition as the result of salt accumulation. This structural change would alter the membrane permeability which, in turn, affects the membrane conductance and the rate of accumulation. The interdependence of these processes can be illustrated in a simple manner:

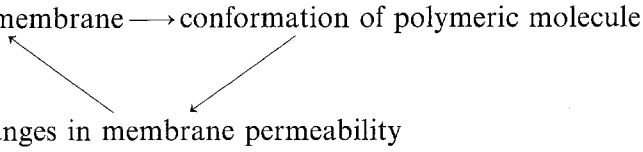

If the processes are coupled in such a way that sufficient feedback is built in, they will continuously reinforce themselves and the system can become unstable.

In mathematical terms, the idea is developed as follows. The salt concentration within the membrane, C_s, is assumed to depend upon current flow I, and membrane permeability which is related to mem-

brane polymer concentration C_m (monomoles/cm^3). Thus, in the steady state,

$$C_s = F(C_m, I). \tag{1}$$

The membrane conformation in turn is related to the salt concentration:

$$C_m = G(C_s). \tag{2}$$

Modeling the time dependence of these two functional relations as first order processes, we have

$$\dot{C}_s = -\chi(C_s - F(C_m)) \quad \text{(with } I = \text{constant)} \tag{3}$$

and

$$\dot{C}_m = -\zeta(C_m - G(C_s)) \tag{4}$$

in which both constants χ and ζ are positive. To study the dynamic properties around the steady state, we perturb C_s^0 and C_m^0 slightly to $C_s^0 + \delta C_s$, $C_m^0 + \delta C_m$. The time derivative of δC_s, δC_m are found to be

$$\delta \dot{C}_s = \frac{d}{dt}(C_s - C_s^0) \equiv -\chi \left(\delta C_s - \left(\frac{\partial F}{\partial C_m} \right)_0 \cdot \delta C_m \right) \tag{5}$$

$$\delta \dot{C}_m = \frac{d}{dt}(C_m - C_m^0) = -\zeta \left(\delta C_m - \left(\frac{\partial G}{\partial C_s} \right)_0 \cdot \delta C_s \right). \tag{6}$$

The solutions of these equations are then

$$\delta C_s = a_1 e^{\lambda_1 t} + b_1 e^{\lambda_2 t}$$

$$\delta C_m = a_2 e^{\lambda_1 t} + b_2 e^{\lambda_2 t}$$

where λ_i are the roots of the determinant

$$\begin{vmatrix} -\chi - \lambda & \chi \left(\dfrac{\partial F}{\partial C_m} \right)_0 \\ \zeta \left(\dfrac{\partial G}{\partial C_s} \right)_0 & -\zeta - \lambda \end{vmatrix} = 0. \tag{7}$$

If the perturbations δC_s and δC_m increase with time, namely either λ_1 or λ_2 have positive real parts, the process will be unstable. From Eq. (7), we obtain

$$\lambda = \tfrac{1}{2}(-\chi - \zeta) \pm \tfrac{1}{2} \sqrt{(\chi + \zeta)^2 + 4\chi\zeta \left(\left(\frac{\partial F}{\partial C_m} \right)_0 \cdot \left(\frac{\partial G}{\partial C_s} \right)_0 - 1 \right)}.$$

For one positive, real root, the condition

$$\left(\frac{\partial F}{\partial C_m} \right)_0 \cdot \left(\frac{\partial G}{\partial C_s} \right)_0 > 1 \tag{8}$$

must be fulfilled.

Explicit expressions for $F(C_m, I)$ and $G(C_s)$ are developed next. According to phenomenological equations, the steady flow of counterions, J_+ and co-ions J_- across the composite membrane are related to the difference of electrochemical potential $\Delta\tilde{\mu}_j^i$ (in which subscript j represents the type of ions, and superscript i refers to the layer, namely α or β) through the expression:

$$J_+^i = \omega_+^i \bar{C}_+^i (\Delta\mu_+^i + F\Delta\psi^i) \tag{9a}$$

$$J_-^i = \omega_-^i \bar{C}_-^i (\Delta\mu_-^i - F\Delta\psi^i) \tag{9b}$$

where $\Delta\tilde{\mu}_j^i$ is expressed as a sum of the difference in chemical potential $\Delta\mu_j^i$ and the difference in electrical potential $\Delta\psi^i$. $\bar{C}_j^i$ is the average concentration, i.e.,

$$\bar{C}_j^i = \left(\frac{1}{\delta^i}\int_{\delta^i}\frac{dx}{C_j^i}\right)^{-1} \quad \text{and} \quad \omega_j^i = \frac{u_j^i}{\delta^i}$$

C_j^i and u_j^i are concentration, mobility of jth ions in ith layer; δ^i represents the thickness of these layers. To express ion flow J_j^i in terms of current, the relation $I = F(J_+^i - J_-^i)$ for single electrolyte is introduced. After cancellation of $\Delta\psi^i$, Eqs. (9) become:

$$J_+^\alpha \left(1 + \frac{\omega_-^\alpha \bar{C}_-^\alpha}{\omega_+^\alpha \bar{C}_+^\alpha}\right) = -\omega_-^\alpha \bar{C}_-^\alpha (\Delta\mu_+^\alpha + \Delta\mu_-^\alpha) + \frac{I}{F} \tag{10a}$$

$$J_-^\alpha \left(1 + \frac{\omega_-^\beta \bar{C}_-^\beta}{\omega_+^\beta \bar{C}_+^\beta}\right) = -\omega_-^\beta \bar{C}_-^\beta (\Delta\mu_+^\beta + \Delta\mu_-^\beta) + \frac{I}{F}. \tag{10b}$$

With no net fixed charge in β layer, i.e., $\bar{C}_+^\beta = \bar{C}_-^\beta = \bar{C}_s^\beta$, and the assumption $u_+^\beta = u_-^\beta$, Eq. (10b) reduced to

$$2J_+^\beta = \omega^\beta \bar{C}_s^\beta (\Delta\mu_+^\alpha + \Delta\mu_-^\alpha) + \frac{I}{F}. \tag{11}$$

At steady state, the flux of jth ion is identical throughout different layers. Hence

$$J_+^\alpha = J_+^\beta. \tag{12}$$

Making use of relation (11), (12), Eq. (10*a*) gives

$$\Delta\mu_+^\alpha + \Delta\mu_-^\alpha = \frac{1 - \left(\dfrac{\omega_-^\alpha \bar{C}_-^\alpha}{\omega_+^\alpha \bar{C}_+^\alpha}\right)}{\omega^\beta \bar{C}_s^\beta \left(1 + \left(\dfrac{\omega_-^\alpha \bar{C}_-^\alpha}{\omega_+^\alpha \bar{C}_+^\alpha}\right)\right) + 2\omega_-^\alpha \bar{C}_-^\alpha} \cdot \left(\frac{I}{F}\right). \tag{13}$$

In case of ideal solution, $\Delta\mu_j^i$ may be expressed in terms of ionic concentration:

$$\Delta\mu_j^\alpha = RT \ln \frac{C_j^{(3)}}{C_j^{(2)}} \tag{14a}$$

$$\Delta\mu_j^\beta = RT \ln \frac{C_j^{(5)}}{C_j^{(4)}}. \tag{14b}$$

As the conditions of Donnon equilibrium are fulfilled at the phase boundary, and $C_+^{(1)} = C_-^{(1)} = C_+^{(6)} = C_-^{(6)} = C_s^B$, we find $\Delta\mu_+^\alpha + \Delta\mu_-^\alpha = \Delta\mu_+^\beta + \Delta\mu_-^\beta$. The left hand of Eq. (13) now reduces to the form $2RT \ln C_s^{(4)}/C_s^{(5)}$ or $2RT(C_s^{(4)} - C_s^{(5)})/\tilde{C}_s^\beta$ (Eq. 15) where $\tilde{C}_s^\beta$ is defined as $(C_s^{(5)} - C_s^{(4)})/(\ln C_s^{(5)} - \ln C_s^{(4)})$. To obtain an expression for average C_s^β as a function of $\frac{I}{F}$ and polymer concentration C_m^α, we eliminate C_+^α, C_-^α from Eq. (13) by employing again the Donnon equilibrium at the phase boundary and the requirements of electroneutrality in α layer. Thus

$$(C_+^{(3)} \cdot C_+^{(2)}) \cdot (C_-^{(3)} \cdot C_-^{(2)}) = (C_s^{(4)} \cdot C_s^{(5)})^2. \tag{16}$$

With a definition of geometric mean average concentration

$$\langle C_j^\alpha \rangle = \sqrt{C_j^{(3)} \cdot C_j^{(2)}}, \quad \langle C_s^\beta \rangle = \sqrt{C_s^{(4)} \cdot C_s^{(5)}} \quad \text{and} \quad \langle C_+^\alpha \rangle = C_m + \langle C_-^\alpha \rangle,$$

Eq. (16) becomes

$$(C_m + \langle C_-^\alpha \rangle)\langle C_-^\alpha \rangle = \langle C_s^\beta \rangle^2$$

or

$$\langle C_-^\alpha \rangle = \tfrac{1}{2}(-C_m + \sqrt{C_m^2 + 4\langle C_s^\beta \rangle^2}), \quad \langle C_+^\alpha \rangle = \tfrac{1}{2}(C_m + \sqrt{C_m^2 + 4\langle C_s^\beta \rangle^2}). \tag{17}$$

When the concentration difference across α and β layer is small, $\bar{C}_j^i \simeq \tilde{C}_j^i \simeq \langle C_j^i \rangle$. Upon introduction of Eq. (17) and assumption $\omega_+^\alpha = \omega_-^\alpha = \omega^\beta = \omega$, Eq. (13) yields the desired form

$$\bar{C}_s^\beta - C_s^B = \frac{-C_s^B + \sqrt{(C_s^B)^2 + \frac{1}{4}\left(C_m^2 + C_m \cdot \frac{I}{RT\omega F}\right)}}{C_m + \frac{I}{RT\omega F}} \cdot \frac{I}{2RT\omega F}. \tag{18}$$

For the case of a membrane of low charge density (i.e., $C_m \simeq 0$), or zero current ($I = 0$), Eq. (18) reduces to $\bar{C}_s^\beta = C_s^B$. The salt accumulation (or depletion) phenomenon disappears. This result is expected, since under these conditions, a difference in transference number no longer exists.

The next expression to be developed is function $G(C_s)$. Let us view the membrane macromolecules as flexible chains each composed of P_s "statistical segment". The average configuration of the molecules is determined by electrostatic interaction between polymeric fixed charges, the screening effect of added electrolyte as well as the osmotic force generated by the more concentrated distribution of counterions in the vicinity of polymeric chains. As first introduced by Kuhn [15], each segment consists of n_s successive monomeric units linked together into a rigid unit of length l, and can rotate in a complete unrestricted fashion about the segment joint. We assume that each segment can only be characterized by one of the two conformational states – either long or short – with regards to the projection of this segment upon end to end axis of the entire molecule. More speficically, the long and short projected length are given as

$$\ell_\ell = \frac{h_{\max}}{P_s}, \qquad \ell_s = \frac{h_{\min}}{P_s} \tag{19}$$

in which $h_{\max}$ and $h_{\min}$ are the maximum and minimum end to end length of the polymeric chain. Hence the end to end distance of the polymer is

$$h = [\ell_s \gamma + \ell_\ell (1-\gamma)] P_s. \tag{20}$$

Where γ is the fraction of segments in the short state. Note that the statistical segment lengths ℓ_ℓ, ℓ_s, as used here are extended somewhat from Kuhn's original definition, since in his case $\ell = \frac{h_{\max}}{P_s}$, a fixed value. Moreover, the two states considered in our model do not necessarily correspond to the helix and coil forms of polyglutamic acid. Potentiometric titration and light scattering studies indicate that in neutral solution (pH = 6.5–7.0), such as that used in our experiments, the helical content of polyglutamic acid is quite small [7]. Thus, it is more appropriate to conceive the polyelectrolyte molecules as transforming from an expanded coil into a tightly coiled configuration with the increasing ionic strength of the solution.

The evaluation of the membrane conformation $G(C_s)$ is based on energetic considerations. The free energy of a macromolecule F_m can be represented by the sum of the free energy of each state times the fraction of the segments in that specific state, plus the free energy of mixing of the two states:

$$F_m = P_s[A\gamma + B(1-\gamma) + kT(\gamma \ln \gamma + (1-\gamma)\ln(1-\gamma))] \tag{21}$$

where A and B are the free energy per segment of short and long states, respectively, k the Boltzman constant. The most probable conformation for the polyelectrolyte molecules under a given ionic environment is that with the minimum energy. Namely

$$\frac{dF_m}{d\gamma}=P_s\left(A-B+kT\ln\frac{\gamma}{1-\gamma}\right)=0.$$

Hence,

$$\gamma=\frac{1}{1+\exp\left(\frac{A-B}{kT}\right)}. \tag{22}$$

$(A-B)$, the change in free energy accompanying the transition from short to long state, is composed of the following term:

(a) Changes in Electrical Energy (ΔE_e)

Assuming that the charge $P\cdot\varepsilon$ carried by the polymer is evenly distributed along the chain, the average charge on each segment is therefore $\frac{P\cdot\varepsilon}{P_s}$ (p=number of polymerization, ε=electronic charge on each monomer). According to Debye-Huckel theory, the potential of the statistical segment, r distance apart from ith segment, assumes the form

$$\Phi=\frac{P\cdot\varepsilon}{P_s}\cdot\frac{e^{-\kappa r}}{D_e r} \tag{23}$$

where D_e is the effective dielectric constant of the medium, κ is the Debye-Huckel reciprocal radius, defined as

$$\kappa=\frac{N_{av}\cdot 4\pi\Sigma C_j\varepsilon^2}{D_e kT}, \tag{24}$$

N_{av} being the Avagadro's number, C_i being the concentration of free ions in the vicinity of polymeric molecules. Thus the electric energy contributed by the two segments is

$$E_e=\tfrac{1}{2}\cdot\frac{P\cdot\varepsilon}{P_s}\cdot d\cdot\Phi \tag{25}$$

where d is the effective degree of ionization. Introducing (23) into (25), we find that the corresponding change of electrical energy during the transition of two states is

$$\Delta E_e = \tfrac{1}{2} \cdot \frac{p^2 \cdot \varepsilon^2}{D_e \cdot P_s^2} \left(\frac{d_s e^{-\kappa_s r_s}}{r_s} - \frac{d_\ell e^{-\kappa_\ell r_\ell}}{r_\ell} \right). \tag{26}$$

Here r_s is the average charge separation between the segments in short state, r_ℓ is that of the long state.

(b) Changes in Energy Arising from Osmotic Pressure Difference (ΔE_π)

The accumulation of salt in the membrane phase tends to increase its osmotic pressure. The energy change as a result of the osmotic variation for the total system is

$$(\Delta E_\pi)_T = -\int_{V_{\ell\ell}}^{V_{\ell_s}} \pi \, dV \tag{27}$$

where dV is the volume change of a unit area of α region of the membrane, and π is the osmotic pressure difference between α and β. Neglecting the nonideality of the solution, π is given by

$$\pi = RT[(\bar{C}_+^\alpha + \bar{C}_-^\alpha) - (\bar{C}_+^\beta + \bar{C}_-^\beta)]. \tag{28}$$

Making use of Eq. (17) and expressing V in terms of C_m $\left(\text{i.e., } V = \frac{\sigma_p \cdot P}{N_{av} \cdot C_m}\right)$, we get

$$(\Delta E_\pi)_T = -\int_{C_{\min}}^{C_{\max}} \frac{\sigma_p \cdot P}{N_{av}} RT(\sqrt{C_m^2 + 4(\bar{C}_s^\beta)^2} - 2\bar{C}_s^\beta) \cdot \frac{-dC_m}{C_m^2} \tag{29}$$

in which $C_{\min}$, $C_{\max}$ correspond to the macromolecular concentration with the segments totally in the long and short states; σ_p is the number of polymeric chains per unit area of the membrane. Henceforth $\bar{C}_s^\beta$ will be written simply as C_s. The average change per segment is therefore

$$\Delta E_\pi = \frac{(\Delta E_\pi)_T}{\sigma_p \cdot P_s}.$$

(c) Changes in Standard Free Energy (ΔE_s)

A neutral polymer molecule, in the equilibrium state, maintains a predominantly coiled configuration. When the molecule is ionized, it extends and is distorted from its most probable entropic configuration as

a result of the additional electrostatic component. The energy difference associated with the variation of this entropy contribution for the coiled and extended molecules is included in this term.

The free energy change is computed from a neutral reference state in which 99.9 % of segments are assumed to be in the short state. With $\gamma = 0.999$, one may find $\Delta E_s = -9\,kT$ from Eq. (22) while setting ΔE_e and ΔE_π to zero since the reference molecule is neutral.

Summing up the terms, the change in free energy for each segment is given by

$$A - B = \Delta E_e + \Delta E_\pi + \Delta E_s. \tag{30}$$

The dependence of C_m on C_s now can be obtained from the expression of free energy difference $(A–B)$ (Eq. 30), the value of γ (Eq. 22), and the definition of C_m (namely, $(\sigma_p \cdot P)/(N_{av} \cdot h)$ Eq. (31)).

The characteristics of the coupling between the diffusional flow $F(C_m, I)$, and membrane conformation $G(C_s)$ is illustrated by means of a numerical example. The parameters chosen in this case fall within the range of our experimental system. The degree of polymerization of the polyglutamic acid is about 5400. With the empirical assignment of n_s (number of monomers per statistical segment) being 4 for a polymethylene chain [22], n_s for polyglutamic acid is assumed to be 6, since this macromolecule has a moderate bulky side chain and is relatively stiff. In a typical polymer of $(-C-CR_1R_2-)$ type, the bond length is found to be 2.0–2.7 Å [22]. Thus the length of monomeric unit in the direction of end to end axis of the molecule $b = 2.4$ Å. The maximum extension of statistical chain element $\ell_\ell (= n_s \times b)$ becomes 14.4 Å. With these values, Eq. (19) gives $h_{\min} = 432$ Å, and $\ell_s = 0.48$ Å. As the result of surface interaction between polymer and Ca^{++}, the macromolecules are assumed to pack rather densely in the matrix, so that the chain density $\sigma_p = 1.44 \times 10^{12}/\text{cm}^2$ which corresponds to one polymer chain per 8.4 Å^2. Thus, $C_{\max} = 3.0$ monomole/liter, and $C_{\min} = 0.1$ monomole/liter according to Eq. (31). If the average charge separation for extended and shortened states are say 5 Å and 3 Å, respectively, then

$$\left(\frac{1}{\kappa}\right)_s = 1.93\,\text{Å} \qquad (\text{with } C_m = 3.0\ \text{M/liter},\ C_s = 2.0\ \text{M/liter})$$

$$\left(\frac{1}{\kappa}\right)_1 = 13.70\text{Å} \qquad (\text{with } C_m = 0.1\ \text{M/liter},\ C_s = 0.0\ \text{M/liter}).$$

Using $D_e = 80$, $d_1 = 0.9$, $d_2 = 1.0$, the electrostatic energy difference given in Eq. (26) is $\Delta E_e = 0.26\,kT$. Since ΔE_e is much smaller than ΔE_s and

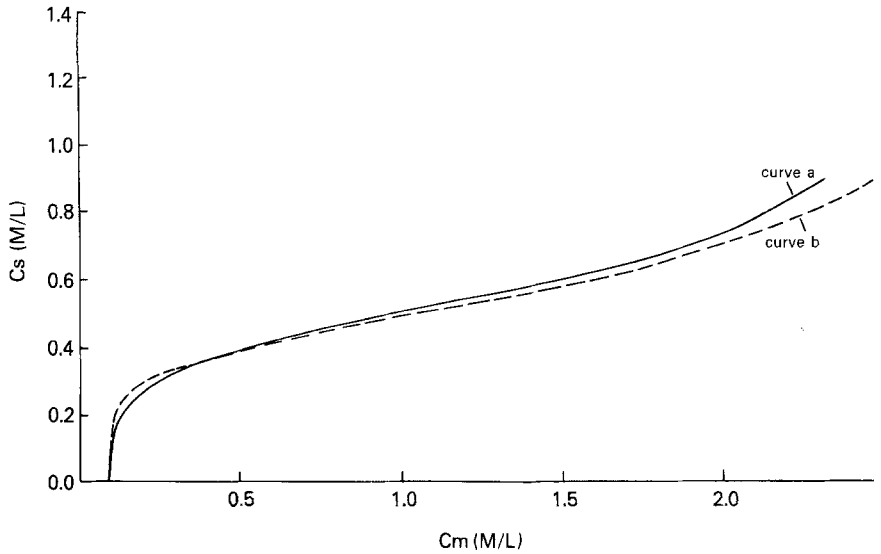

Fig. 8(*a*). The dependence of the membrane concentration C_m upon C_s. The difference between curve *a* and curve *b* is that the cooperativity is included in the latter curve

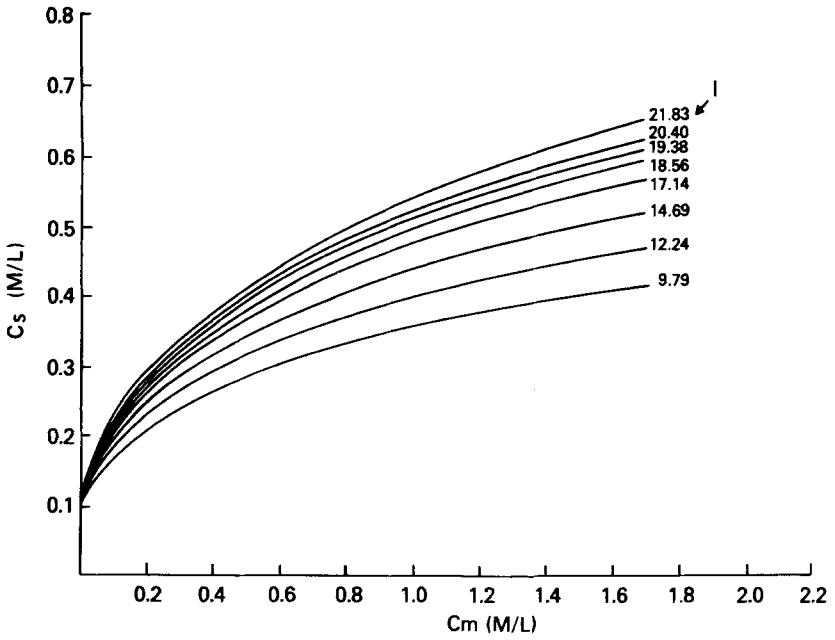

Fig. 8(*b*). The functional relation between C_s and C_m for various current values

ΔE_π, the contribution of ΔE_e to A–B is therefore neglected in our numerical calculation. Numerically solving Eqs. (30), (22), (31) for various values of C_s, the dependency of C_m on C_s is obtained (curve *a* in Fig. 8*a*).

It is interesting to note that, in the region 0.25–0.60M/liter, a small variation of C_s causes a relatively large change in C_m. This steep function emerges without introducing the concept of cooperativity. Membrane excitation has been modelled in terms of cooperative transition of constituent units [2]. As we will see later, however, cooperativity is not a necessary condition for the occurrence of the instability in the complex membrane system. For the sake of comparison, we have, in another calculation, included a cooperative effect in the energetic expression using a somewhat smaller value for $\Delta E_s(=-8kT)$. Instead of Eq. (22), the fraction of segments in the short state is then described by

$$\gamma=\frac{1}{1+\exp\dfrac{(A-B+\eta\gamma)}{kT}} \tag{32}$$

where η is the free energy accounting for the cooperative properties of the polymers. For this calculation, η is assumed to be $1.0kT$. The dependence of membrane polymer concentration C_m upon C_s, including the cooperativity is given in Fig. 8*a* (curve *b*). The general shape of curve *b* is very similar to curve *a* with, as one would expect, the transition between the states becoming a slightly steeper function.

We now calculate C_s as a function of C_m from Eq. (18) using the same values of $C_{\max}$ and $C_{\min}$. Since the polyelectrolyte layer has a tight structure, a small value for ω $(=5\times10^{-15}(\text{cm}\cdot\text{mole})/(\text{erg}\cdot\text{sec}))$ is assigned. The functional relation between C_s and C_m for various I is given in Fig. 8*b*. As shown here, C_s increases moderately with C_m, leveling off for values of C_m greater than about 0.5M/liter. With increasing I, C_s becomes a steeper function of C_m. To study the coupling between salt accumulation and conformational changes of macromolecules, we combine curves *a* and *b* of Fig. 8*a* with Fig. 8*b* in the composite plots (Fig. 9*a* and *b*). The crossing points of the curves, labelled *a* to *i* (Fig. 9*a*), or *a* to *p* (Fig. 9*b*) represent the steady states of the system. These steady-state points can be categorized into two types: unstable and stable. For current ranges 18.56 to 20.40 ma/cm^2 (Fig. 9*a*), curves $F(C_m, I)$ cross curve *a* more than once, whereas only a single intersection exists for curves with current density outside this range.

Since at point *a*, $\dfrac{\partial F}{\partial C_m}<\dfrac{1}{\left(\dfrac{\partial G}{\partial C_s}\right)}$ this steady state is stable. Similarly states *b*, *c*, *d*, *e*, *f*, *h*, *i*, *j* are all stable states. At point *g*, on the other hand,

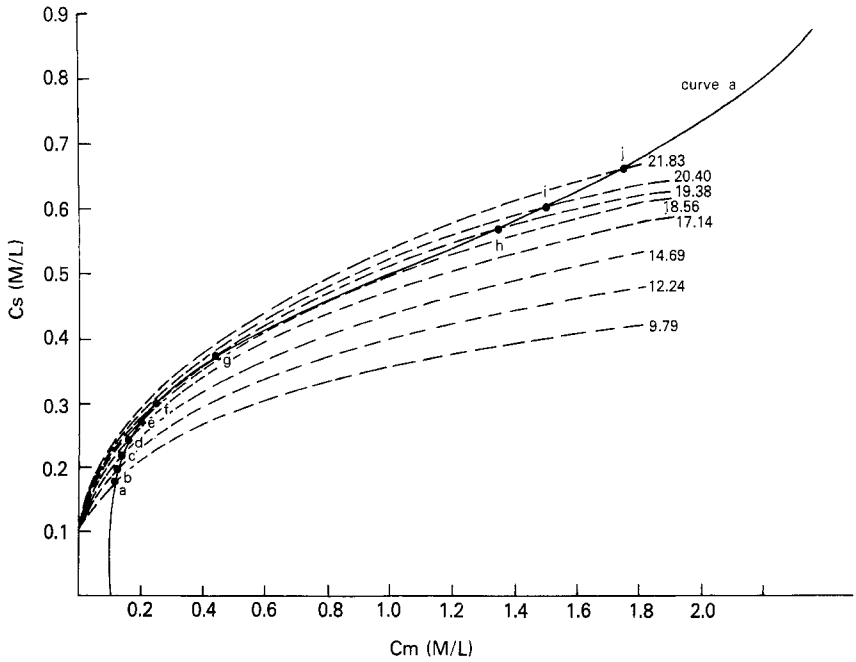

Fig. 9(*a*). A composite plot of Fig. 8*a*, curve *a*, and Fig. 8*b*. The crossing points *a* to *j* are the steady states of the system

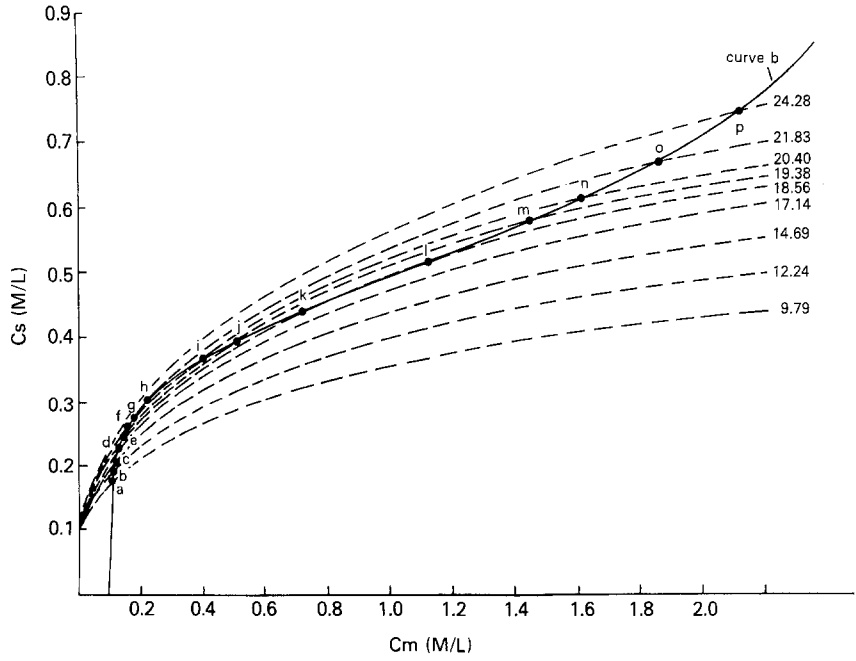

Fig. 9(*b*). A composite plot of Fig. 8*a*, curve *b*, and Fig. 8*b*. Points *a* to *p* are the steady states of system

the product of $\frac{\partial F}{\delta C_m}$ and $\frac{\delta G}{\delta C_s}$ is greater than 1. Any perturbation in C_m will continue to increase in magnitude until an adjacent stable state (either f or h in this case) is reached. Point g is then an unstable state. This steady state is generally unobservable in practice, however, unless C_m is set exactly equal to $(C_m)_g$. Any slight deviation will drive the system away from this state.

Replotting the steady-state values of C_m in Fig. 10*a* as a function of current density, a time independent hysteresis loop is obtained. When we increase current, C_m will increase with it until point f is reached. Further increase in I results in a large increase in C_m. The state point jumps from f to i. From this point on, C_m increases at a much slower rate upon increasing current density. Now if we decrease the current flow, the system will not follow the path $i \rightarrow f \rightarrow e \rightarrow a$ as expected in a reversible process. Instead, the membrane macromolecules remain in coiled conformation (state h) which corresponds to relatively large C_m, until sufficient small ions leave the membrane. It is only then the decreasing osmotic energy of the system surmount the increasing standard (or entropic) energy and C_m will start to return to state e. A hysteresis cycle is evolved through the coupling of ion accumulation and the conformational changes of polyelectrolyte in membrane.

Similar analysis is undertaken for Fig. 9*b* in which the effect of cooperativity is taken into consideration. The general feature of the hysteresis phenomenon (Fig. 10*b*) closely resemble that in Fig. 10*a* except the unstable region covers a wider range of current (17.1–21.8 ma/cm^2).

Discussion

The biological membrane, far from being merely a static barrier separating the interior of the cell from its surrounding environments, is a dynamic entity in which its structure and function are closely related. The coupled salt accumulation and two states macromolecular conformation model examined here provides an example for the correlation between the development of dynamic phenomenon and the structural change of the membrane, and gives a plausible explanation for the observations in polyglutamic acid-calcium membrane. Our model is similar to the models proposed by Tasaki *et al.* [23], and by Baumann *et al.* [1], in that the excitation processes are the result of changes of conformation of the constituent molecules which, in turn, alter the

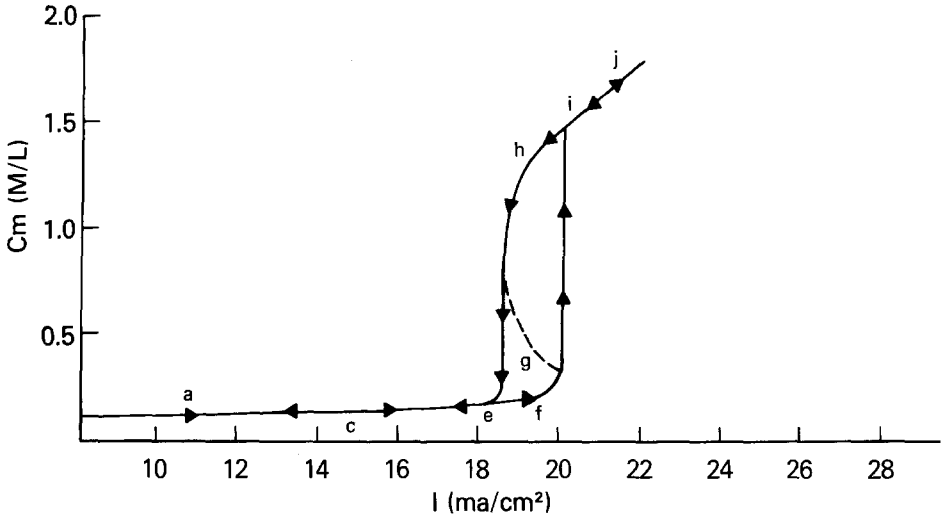

Fig. 10(*a*). Hysteresis loop emerges from replotting C_m in Fig. 9*a* in terms of current I, the labels a to j correspond to the steady state points in Fig. 9*a*. Dotted line indicates the unstable region

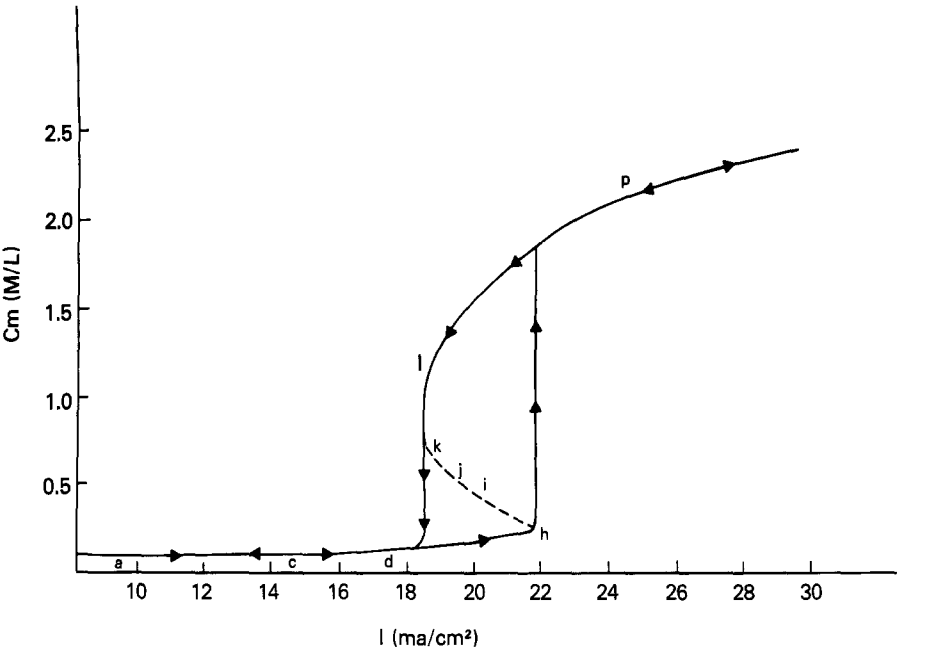

Fig. 10(*b*). Similar plot as Fig. 10*a* except the points correspond to the steady states in 9*b*

permeability of the transporting ions through the membrane. The major difference among these various models lies in the different mechanisms postulated for the conformational transformations.

In our calculation, the character of the time-dependent process is studied from steady-state analysis. Emphasis is placed upon the existence of instability arising from coupling between the membrane structure and the ionic environment. Many simplified assumptions and approximations have been made in the analysis, e.g., the cross coupling coefficients between ionic flows (Eq. (9)) were set to zero. In spite of these simplications, however, qualitative characteristics similar to those observed emerge from the calculations.

From such treatment, we are able to establish the range of current in which hysteresis occurs. In the polyglutamic-calcium membrane, the hysteresis cycle is observed between 5.1 and 26.4 ma/cm^2. The theoretical hysteresis loop lies in the relatively narrow current range: 18.5–20.4 ma/cm^2 (Fig. 10*a*). The theoretical values fall within the correct range of experimental observations. When weak cooperativity in the conformational change is included in the calculations, the theoretical hysteresis loop is found in the current range between 17.1–21.8 ma/cm^2 (Fig. 10*b*). While better agreement between theory and experiment is obtained in the latter case, cooperativity is not essential to the manifestation of hysteresis. Thus, within the approximate framework of our analysis, we cannot conclude whether cooperative transformation of macromolecules indeed exists in the experimental system.

The theory also indicates that conformation of membrane macromolecules has to be a sensitive function of electrolyte concentration to give rise to the dynamic behavior in our system. As shown in the analysis, the system becomes unstable when the product $\frac{\partial F}{\partial C_m} \cdot \frac{\partial G}{\partial C_s}$ is greater than unity. In order to have this condition fulfilled, there must be in $G(C_s)$ a region where C_m varies steeply with C_s. As in Fig. 9*a*, this steep slope results in a large $\frac{\partial G}{\partial C_s}$ at point g, and $\frac{\partial F}{\partial C_m} \cdot \frac{\partial G}{\partial C_s} > 1$; hence instability of the steady state results. It is of interest to note that in excitable biological membranes such as those of nerve or muscle, the steady-state conductance is a steep function of membrane potential. This characteristic results in the negative conductance in the current voltage relation and instability of the systems [8]. The direct relation between the polyelectrolyte conformation and the conductance in our model membrane surely exists although quantitative evaluation between these two parame-

ters is rather difficult and has not been attempted here. Such evaluation should be possible, and could then lend some insights into the mechanism of the excitation phenomena observed in biological systems.

We have made a rough estimation for the time constant of salt accumulation by means of Fick's law [9]. The time constant τ has the form $\frac{2\delta^2}{\pi^2 D}$ in which δ is the thickness of β layer, D the diffusion coefficient of ions in membrane phase. Assuming $\delta = 2000$ Å, we find $\tau = 32$ msec. Interestingly, the rate of accumulation is the same order of magnitude as the frequency of oscillation. The response time of small ion redistribution within the membrane matrix as results of current flow and macromolecule conformation is in the appropriate range to account for the observed periodicity.

In this work we illustrate the role that modification of membrane structure and salt accumulation may play in the occurrence of instability of the membrane. Detailed analysis of relaxation data is not given here. Further study of kinetics of polymer conformation in this model membrane will be useful in correlating the empirical results and our theoretical conclusions.

We would like to thank Dr. V.E.Shashoua for his valuable advice concerning the preparation of polyelectrolyte membrane. The work is supported by NIH Grant No. 5T01 GM 00718.

This paper has been submitted to the Faculty of Graduate School of SUNY, Buffalo, in partial fulfillment of requirement for the degree of Doctor of Philosophy.

References

1. Baumann, G., Mueller, P. 1974. A molecular model of membrane excitability. *J. Supramol. Struct.* **2**:538
2. Blumenthal, R., Changeux, J.P., Lefever, R. 1970. Membrane excitability and dissipative instabilities. *J. Membrane Biol.* **2**:351
3. Cherry, R.J., Chapman, D., Graham, D.E. 1972. Studies of the conductance changes induced in bimolecular lipid membranes by alamethicin. *J. Membrane Biol.* **7**:325
4. Ehrenstein, G., Lecar, H., Nossal, R. 1970. The nature of the negative resistance in bimolecular lipid membranes containing excitability inducing material. *J. Gen. Physiol.* **55**:119
5. Eisenberg, M., Hall, J.E., Mead, C.A. 1973. The nature of the voltage-dependent conductance induced by alamethicin in black lipid membranes. *J. Membrane Biol.* **14**:143
6. Gordon, L.G.M., Haydon, D.A. 1972. The unit conductance channel of alamethicin. *Biochim. Biophys. Acta* **225**:1014
7. Hawkins, R.B., Holtzer, H. 1972. Some macromolecular properties of poly (α-L-glutamic acid) random coil. *Macromolecules* **5**:294

8. Hodgkin, A.L., Huxley, A.F. 1972. Quantitative description of membrane current and its application to conduction and excitation in nerve. *J. Physiol. (London)* **117**:550
9. Huang, L.M. 1975. Dynamic Properties of a Polyelectrolyte Calcium Membrane. PhD. Dissertation, SUNY at Buffalo, Buffalo
10. Jones, G.T., Lewis, T.J. 1975. Current oscillations in iodine-doped polyethylene film. *Faraday Symp. Chem. Soc.* **9**:192
11. Katchalsky, A. 1964. Polyelectrolytes and their biological interactions. *Biophys. J.* **4(Suppl.)**:9
12. Katchalsky, A. 1967. Membrane thermodynamics. *In:* The Neuroscience: A Study Program. Rockefeller University Press, New York
13. Katchalsky, A., Alexandrovitch, Z., Kedem, O. 1966. The dynamics of macromolecular systems. *In:* Chemical Physics of Ionic Solutions. B.E. Conway and R.G. Barradas, editors Wiley, New York
14. Katchalsky, A., Spangler, R.A. 1968. Dynamics of membrane processes. *Q. Rev. Biophys.* **1**:127
15. Kuhn, W. 1934. Über die Gestalt fadenförmiger Moleküle in Lösungen. *Koll. Z.* **68**:2
16. Lehninger, A.L. 1970. Biochemistry. Worth, New York
17. Mueller, P., Rudin, D.O. 1968. Action potentials induced in bimolecular lipid membranes. *Nature (London)* **217**:713
18. Muller, R.U., Finkelstein, A. 1972. Voltage-dependent conductance induced in thin lipid films by monazomycin. *J. Gen. Physiol.* **60**:263
19. Shashoua, V. 1967. Electrically active polyelectrolyte membrane. *Nature (London)* **215**:846
20. Shashoua, V. 1969. Electrically active protein and polynucleic acid membrane. *In:* Molecular Basis of Membrane Function. D.C. Tosteson, Editor. Prentice Hall, Englewood
21. Shashoua, V. 1975. Electrical oscillatory phenomena in protein membranes. *Faraday Symp. Chem. Soc.* **9**:174
22. Tanford, C. 1961. Physical Chemistry of Macromolecules. Wiley, New York
23. Tasaki, I., Kobatake, Y. 1967. Nerve Excitation. Charles C. Thomas, Springfield, Ill.
24. Teorell, T. 1959. Electrokinetic membrane processes in relation to properties of excitable tissues. 1. Experiments on oscillatory transport phenomena in artificial membrane. *J. Gen. Physiol.* **42**:831
25. Teorell, T. 1959. Elektrokinetic membrane processes in relation to properties of excitable tissues. 2. Some theoretical considerations. *J. Gen. Physiol.* **18**:847
26. Yoshida, M., Kamo, N., Kobatake, Y. 1972. Transport phenomena in a model membrane accompanying a conformational change: Membrane potential and ion permeability. *J. Membrane Biol.* **8**:389